

1                   **Historic carbon burial spike in an Amazon floodplain lake linked to riparian**  
2                   **deforestation near Santarem, Brazil**

3

4   Luciana M. Sanders<sup>1</sup>, Kathryn Taffs<sup>1</sup>, Debra Stokes<sup>2</sup>, Christian J. Sanders<sup>3</sup>, Alex Enrich-  
5   Prast<sup>4,5</sup>, Leonardo Nogueira Amora<sup>6,7</sup>, Humberto Marotta<sup>6,7</sup>

6

7

8

9   <sup>1</sup>*Southern Cross Geoscience, Southern Cross University, P.O. Box 157, Lismore, NSW 2480, Australia.*

10   <sup>2</sup>*Marine Ecology Research Centre, Southern Cross University, P.O. Box 157, Lismore, NSW 2480,  
11                   Australia University, P.O. Box 157, Lismore, NSW 2480, Australia.*

12   <sup>3</sup>*National Marine Science Centre, School of Environment, Science and Engineering, Southern Cross  
13                   University, Coffs Harbour, New South Wales, Australia.*

14   <sup>4</sup>*Laboratório de Biogeocíquímica, Universidade Federal do Rio de Janeiro (UFRJ), Rio d Janeiro (RJ),  
15                   21941 971, Brazil.*

16   <sup>5</sup>*Department of Environmental Change, Linköping University, 581 83, Linköping, Sweden.*

17   <sup>6</sup>*Ecosystems and Global Change Laboratory (LEMG-UFF) / International Laboratory of Global Change  
18                   (LINCGlobal). Biomass and Water Management Research Center (NAB-UFF). Graduated  
19                   Program in Geosciences (Environmental Geochemistry). Universidade Federal Fluminense  
20                   (UFF), Av. Edmundo March, s/nº – Zip Code: 24210-310, Niteroi/RJ- Brazil.*

21   <sup>7</sup>*Sedimentary and Environmental Processes Laboratory (LAPSA-UFF). Department of Geography.  
22                   Graduated Program in Geography. Universidade Federal Fluminense (UFF), Av. Gal. Milton  
23                   Tavares de Souza, s/nº - Zip Code: 24210-346, Niteroi/RJ- Brazil.*

24

25

26

27

28   \*Corresponding author. E-mail address; [l.sanders.13@student.scu.edu.au](mailto:l.sanders.13@student.scu.edu.au)

29

30

31

32      **Abstract**

33      The forests along the Amazon Basin produce significant quantities of organic  
34      material, a portion of which is deposited in floodplain lakes. However, potentially  
35      important effects of ongoing deforestation in the watershed on these carbon fluxes is still  
36      poorly understood. Here, a sediment core was extracted from an Amazon floodplain lake  
37      to examine the relationship between carbon burial and land cover/use. Historical records  
38      from 1934 and satellite data from 1975 were used to calculate deforestation rates between  
39      1934 and 1975, and 1975 to 2008 in four zones with different distances from the margins  
40      of the lake and its tributaries (100, 500, 1000 and 6000-m buffers). Sediment  
41      accumulation rates were determined from the  $^{240+239}\text{Pu}$  signatures and the excess  $^{210}\text{Pb}$   
42      method, reaching near 3.8 and 4.2 mm year $^{-1}$  in the last 60 and 120 years respectively.  
43      The carbon burial rates ranged between 81 and 284 g C m $^{-2}$  year $^{-1}$ , with pulses of high  
44      carbon burial derived from the forest vegetation, as indicated by  $\delta^{13}\text{C}$  and  $\delta^{15}\text{N}$  signatures  
45      in the 1940s and 50s. Finally, our results revealed a potentially important spatial  
46      dependence of the OC burial in Amazon lacustrine sediments in relation to deforestation  
47      rates in the catchment. These deforestation rates were more intense in the riparian  
48      vegetation (100-m buffer) during the period 1934-1975 and the larger open water areas  
49      (500, 1000 and 6000-m buffer) during 1975-2008. The continued removal of vegetation  
50      from the interior of the forest was not related to the peak of OC burial in the lake, but  
51      only the riparian deforestation which peaked during the 1950s. Our novel findings  
52      suggest the importance of abrupt and temporary events in which some of the biomass  
53      released by the deforestation, especially restricted to areas along open water edges, might  
54      reach the depositional environments in the floodplain of the Amazon Basin.

55

56        **1. Introduction**

57        Rivers act as vectors, transporting sediment from land to ocean (Abril et al. 2014).  
58        Along this trajectory a significant proportion of the sediment load, including organic  
59        material, may be deposited in floodplains, creating zones of carbon accumulation (Smith  
60        et al. 2002, Dong et al. 2012, Hoffmann et al. 2013). This process is accelerated during  
61        flood events, when rivers and tributaries deposit organic material along the inundated  
62        floodplains (Smith et al. 2002). In some climate zones, floodplains are seasonally  
63        inundated, with riparian zone vegetation dependent upon this seasonal influx of organic  
64        material. The riparian vegetation slows water velocity and traps fine-grained, carbon rich  
65        sediments within this low-energy environment (Aalto et al. 2003). Therefore, the riparian  
66        vegetation along the floodplains may be important for the organic matter deposition and  
67        the Amazon carbon cycle.

68        The importance of tropical wetland ecosystems in the carbon cycle is well  
69        documented (Downing et al. 1993, Melack et al. 2004, Zocatelli et al. 2013, Abril et al.  
70        2014, Marotta et al. 2014). It has been shown that wetlands in the warm tropics are some  
71        of the most productive biological communities in the world (Neue et al. 1997),  
72        representing an important sink for nutrients (Marotta et al. 2009) and carbon (Peixoto et  
73        al. 2016), as well as sources of organic substrates to carbon gas production in inland  
74        waters (Marotta et al. 2010). However, these wetland ecosystems are also highly  
75        threatened by land use activities, especially from deforestation, development of  
76        agricultural land and soil degradation (Junk 2013, Lucas et al. 2014). For example, the  
77        Amazon Basin wetlands are being degraded by farming activities such as commercial  
78        ranching, and an increase in road density (Goulding 1993).

79 Deforestation of the Amazon Basin accelerated toward the end of the 1970's  
80 (Skole and Tucker 1993), when an estimated 15% of the pristine rainforest area was lost  
81 by the year 2003, increasing to approximately 18% by 2015 (INPE 2016). The ongoing  
82 loss of vegetation is responsible for a substantial increase in erosion rates and subsequent  
83 sediment inputs into Amazon rivers and lakes (Neill et al. 2013b). Yet these  
84 anthropogenic activities are potential sources of allochthonous organic matter that may  
85 increase carbon stores in the associated floodplain areas (Diaz and Rosenberg 2008,  
86 Stanley et al. 2012).

87 The city of Santarém, in central Amazon, was established in the mid-eighteenth  
88 century, approximately 650 km upstream from the Amazon River mouth and at its  
89 confluence with the River Tapajós (02°25'0.28"S and 54°42'41.57"W, Figure 1). In 1940,  
90 Santarém was only a small village with less than 0.5 km<sup>2</sup>, surrounded by dense pristine  
91 rainforest (estimation from the historical mapping of the Santarém City Hall). This city  
92 quickly expanded, occupying 5.2 km<sup>2</sup> by the end of the 1970s and 49.3 km<sup>2</sup> currently  
93 (estimation from satellite images LANDSAT/SRTM). Jupindá Lake is 70 km East of  
94 from Santarém City, and receives surface water inflow from small streams draining from  
95 the forest and the main tributary Curuá-Una River, a large affluent of the Amazon River  
96 (Figure 1). The Lake has been affected by the deforestation associated with the expansion  
97 of Santarém City. Between the 1940's and 1950's, there was intense deforestation on the  
98 margins of rivers and streams in this area, used to supply the markets with wood and  
99 forestry products (Amorim 2000, Cruz et al. 2011). In the 1970s, the Curuá-Una River  
100 was dammed (Curuá-Una Dam) 45 km upstream of Jupindá Lake to build the first  
101 hydroelectric plant of the Amazon Forest (LigockI 2003).

102 Jupindá Lake provides an ideal opportunity to investigate historical changes in  
103 organic carbon burial in a floodplain lake as a result of the well documented  
104 anthropogenic activities. This will aid in identifying the still-little known impacts of land  
105 cover changes on recent carbon burial rates in depositional environments of the Amazon  
106 floodplain. The objectives of this research are to investigate the affects of deforestation  
107 and urban development on carbon burial rates in a tropical floodplain lake.

108

109 **2. Methods**

110 A 60 cm depth sediment core (diameter 7.5 cm) was collected in 2010 using a  
111 gravity corer in the center of the Jupindá Lake (02°27'43.60" S, 54° 5'1.30" W. The  
112 sediment core was sub sampled at 2 cm intervals. Dry bulk density (DBD, g cm<sup>-3</sup>) was  
113 determined as the dry sediment weight (g) divided by the initial volume (cm<sup>3</sup>). A  
114 homogenized portion was acidified to remove carbonate material, then dried and ground  
115 to powder for organic carbon (OC), nitrogen (N), δ<sup>13</sup>C, and δ<sup>15</sup>N analyses using a Flash  
116 Elemental Analyzer coupled to a Thermo Fisher Delta V IRMS (isotope ratio mass  
117 spectrometer). Analytical precision: C = 0.1 %, N = 0.1%, δ<sup>13</sup>C = 0.1‰ and δ<sup>15</sup>N = 0.15  
118 ‰.

119 Samples were prepared for Pu dating following the method of Ketterer et al.  
120 (2004) with modifications to enable larger sample mass to be processed as a result of the  
121 likely lower Pu concentrations in the Southern Hemisphere (Sanders et al. 2016). To  
122 obtain a larger mass, sediment intervals were joined and homogenized so the sediment  
123 intervals for the <sup>240+239</sup>Pu dating was 4 cm intervals. Sample aliquots ranging from 14 to  
124 29 grams were dry-ashed at 600 °C for 16 hours, and leached with 50 mL of 16 M HNO<sub>3</sub>.

125 The leaching was conducted overnight at 80°C with added  $^{242}\text{Pu}$  yield tracer (NIST  
126 4334g, 19 picograms). Acid leaching (as opposed to complete dissolution with HF) is  
127 known to solubilize stratospheric fallout Pu, and there is little possibility that “refractory”  
128  $\text{HNO}_3$ -insoluble Pu exists in the South America (Sanders et al. 2014). The leachates  
129 were diluted to 100 mL, filtered to remove solids, and the aqueous solutions were  
130 processed with TEVA resin (EIChrom, Lisle, IL, USA) in order to chemically isolate 3.0  
131 mL Pu fractions in aqueous ammonium oxalate solution suitable for measurements by  
132 sector ICPMS. Pu determinations were performed using a VG Axiom MC operating in  
133 the single collector (electron multiplier) mode. The system was used with an APEX HF  
134 desolvating micronebulizer system (ESI Scientific, Omaha, NE, USA) with an uptake  
135 rate of 0.4 mL/minute. Qualitative mass spectral scans (averages of 50 sweeps over the  
136 mass range 237.4 – 242.6) were collected for selected samples prior to the electrostatic  
137 sector quantitative scanning of  $^{238}\text{U}^+$ ,  $^{239}\text{Pu}^+$ ,  $^{240}\text{Pu}^+$ , and  $^{242}\text{Pu}^+$ . Detection limits were  
138 evaluated based upon the analysis of two blanks and considerations regarding the  
139 obtained mass spectra. A detection limit of 0.01 Bq/kg of  $^{239+240}\text{Pu}$  is applicable for  
140 samples of nominal 25 g mass.

141 For  $^{210}\text{Pb}$  dating, an intrinsic germanium detector coupled to a multi-channel  
142 analyzer was used. Freeze dried and ground sediments were packed and sealed in gamma  
143 tubes. Lead-210 and  $^{226}\text{Ra}$  activities were calculated by multiplying the counts per minute  
144 by a factor that includes the gamma-ray intensity and detector efficiency determined from  
145 standard calibrations. Identical geometry was used for all samples. Lead-210 activities  
146 were determined by the direct measurement of the 46.5 KeV gamma peak. Radium-226  
147 activity was determined via the  $^{214}\text{Pb}$  daughter at 351.9 KeV. For  $^{226}\text{Ra}$  measurements,

148 the packed samples were set aside for at least 21 days to allow for  $^{222}\text{Rn}$  to ingrow and  
149 establish secular equilibrium between  $^{226}\text{Ra}$  and its granddaughter  $^{214}\text{Pb}$ . Excess  $^{210}\text{Pb}$   
150 activity was calculated by subtracting the supported  $^{210}\text{Pb}$  (i.e.,  $^{226}\text{Ra}$  activity) from the  
151 total  $^{210}\text{Pb}$  activity. The sediment accretion rate for the previous 120 years was estimated  
152 by two methods derived from  $^{210}\text{Pb}$  dating, the Constant Initial Concentration (CIC)  
153 model assuming that this rate has not varied during the encompassed time span (Appleby  
154 and Oldfield 1992), and the Constant Rate of Supply (CRS) model based on a constant  
155 influx of unsupported, atmospheric  $^{210}\text{Pb}$  that allows a variable sediment rate (Ivanovich  
156 and Harmon 1992). Organic carbon accumulation rates were estimated from an average  
157 between these the two dating methods,  $^{239+240}\text{Pu}$  and  $^{210}\text{Pb}_{\text{ex}}$  the dry bulk density ( $\text{g cm}^{-3}$ )  
158 and carbon content for each interval of the entire sediment core.

159 The land/use cover analysis was based on documented historical information  
160 before 1975 and satellite images (Landsat/SRTM, Table 1) from 1975, 1985, 1995 and  
161 2008 available from the United States Geological Survey (USGS). No significant  
162 deforestation occurred in the catchment area of the Jupindá Lake until early 1940's  
163 (Amorim 2000, Cruz et al. 2011). Subsequent land/use changes were determined using  
164 satellite images (Gordon 1980, Munyati 2000). All satellite images were from low-water  
165 seasons to remove the influence of the flood pulse on the exposed area over years. The  
166 resolution of the images was 30 m, except that from the 1970's which was resampled  
167 from 90 to 30 m (Table 1). This approach allowed an assessment of changes in land cover  
168 which could then be compared to results from carbon accumulation. Results of the  
169 spatial assessment were separated into two time periods; 1934-1975, or the timeframe  
170 between the onset of land clearing and the first satellite image, and 1975-2008 which

171 provides a more detailed assessment of temporal changes to the study area. The time  
172 period 1934-1975 was characterized by a rapid removal (peak until the 1960's) of  
173 vegetation established at the margins of inland waters; especially *Aniba rosaeodora* (Pau-  
174 rosa) for extraction of oils, and *Mezilaurus itauba* and *Cedrela fissilis* (Louro-itaúba and  
175 Cedro, respectively) as hardwoods, and the opening of clearings for crops of textile fibers  
176 and subsistence products. Further, intensification of deforestation towards the interior of  
177 the forest and following the urban growth of Santarém is reported from the 1970's, along  
178 with depleting vegetal resources near to the margins of lakes and running waters in this  
179 region was noted (Amorim 2000, Cruz et al. 2011).

180 In order to address the spatial dependence of recent OC burial in Jupindá Lake for  
181 deforestation, we analyzed the land/cover use in four buffer areas around this lake and  
182 contributing rivers or streams. The first buffer of 100 m represented the riparian forest  
183 protected area by the Brazilian laws for fluvial channels with a width of 50 to 200 m.  
184 Other buffers were progressively higher, with a width of 500, 1000 and 6000 m from the  
185 riverbank and lake margins (Figure 2). In addition, we considered only stretches of rivers  
186 and streams 65-km long from Jupindá Lake to analyze its catchment area of more direct  
187 influence. This criteria also allowed to avoid the interference of the artificial flooding on  
188 the margins of the Curuá-Una hydroelectric dam, which was built in 1977 (Fearnside  
189 2005). All the statistical tests used in this work were performed using GraphPad Prism  
190 5.0 software.

191

192 **3. Results**

193 Analyses of  $^{239+240}\text{Pu}$  were not detectable from the bottom of the sediment core until  
194 the 22-26 cm interval (Figure 3). This radioisotope was detected in the 18-22 cm interval  
195 ( $0.029 \pm 0.002 \text{ Bq/kg } ^{239+240}\text{Pu}$ ) with the highest concentrations ( $0.047 \pm 0.004 \text{ Bq/kg}$   
196  $^{239+240}\text{Pu}$ ) at the 16 cm depth. The  $^{239+240}\text{Pu}$  activities appears to spike at the 14 to 18 cm  
197 interval, which indicates the 1963 stratospheric fallout peak. It may be said with certainty  
198 that the material below 22 cm was deposited pre-bomb (that is, prior to the early 1950's).  
199 This affixes an upper limit on the average sedimentation rate of near to  $3.8 \text{ mm year}^{-1}$ .  
200 The Pu atom ratio data indicate that the Pu is originating from stratospheric fallout  
201 (plutonium isotopic ratios ( $^{240/239}\text{Pu}$ ) of  $\sim 0.18$ ). These results are consistent with the  
202  $^{240}\text{Pu} / ^{239}\text{Pu}$  of  $0.180 \pm 0.014$  discussed by Kelley et al. (1999).

203 The  $^{210}\text{Pb}$  and  $^{226}\text{Ra}$  profiles as well as the  $^{210}\text{Pb}_{(\text{ex})}$  profile vs cumulative dry mass  
204 accumulation reveals a complex depositional environment with sedimentation variations  
205 in the upper intervals with disturbances, such as bio-turbation and resuspension in the  
206 upper  $\sim 20$  cm of the sediment column (Figure 4). A decrease in  $^{210}\text{Pb}_{\text{ex}}$  activity was  
207 found below the 20 cm depth interval. The  $^{210}\text{Pb}_{\text{ex}}$  data distribution are as follows:  $y = -$   
208  $0.0749x + 7.5$ ;  $R^2 = 0.73$ ;  $n=19$ ;  $p < 0.01$  from the 20 to the 60 cm interval, below the  
209 apparent mixed zone. Both estimates of sediment accretion rate during the 120 years from  
210 CIC and CRS models were similar, reaching  $4.1$  and  $4.3 \text{ mm yr}^{-1}$  respectively, which  
211 were slightly higher than the  $\sim 60$  year  $^{239+240}\text{Pu}$  dates ( $3.8 \text{ mm yr}^{-1}$ ). To present the  
212 historical profiles of the carbon burial rates, an average is taken between these the two  
213 dating methods,  $^{239+240}\text{Pu}$  and  $^{210}\text{Pb}_{\text{ex}}$  ( $4 \text{ mm year}^{-1}$ ), multiplied by the DBD and carbon  
214 content for each interval of the entire sediment core.

215 The dry bulk density (DBD), total organic carbon (OC%), total nitrogen (TN%)

216 content as well as the carbon and nitrogen (C/N) molar ratios along with the  $\delta^{13}\text{C}$  and  
217  $\delta^{15}\text{N}$  values showed an increases towards the center of the sediment core Table 2. The  
218 relationship between  $\delta^{13}\text{C}$  and  $\delta^{15}\text{N}$  indicated different origins of OC in the sediment core  
219 (Figure 5) contributing to the significant relationship between recent OC burial and the  
220  $\delta^{13}\text{C}$  (Figure 6). The peak of greater  $\delta^{13}\text{C}$  and lower  $\delta^{15}\text{N}$  values coupled to higher OC  
221 burial rates were observed in the phase between 1934-1975 in Jupindá Lake (one-way  
222 ANOVA followed by Tukey's post test,  $p<0,05$ ; Fig. 7). The  $\delta^{13}\text{C}$  values were around 3  
223 and 5% greater in the phase 1934-1975 in relation to those previous and after respectively  
224 (one-way ANOVA followed by Tukey's post test,  $p<0,05$ ). This peak between 1934-1975  
225 also showed delta  $\delta^{15}\text{N}$  values around 30% lower and OC burial rates around 40 % higher  
226 than other phases (one-way ANOVA followed by Tukey's post test,  $p<0,05$ ).

227 The OC burial rates show an increasing trend from ~ 1930 to 1960 with a peak during  
228 the 1940's and 50's (grey area in Figure 7). The carbon burial rates increased, from ~150  
229  $\text{g m}^{-2} \text{ year}^{-1}$  in the time period 1890 – 1940, and up to  $298 \text{ g m}^{-2} \text{ year}^{-1}$  between 1940 and  
230 1950. Carbon accumulation then decreased to approximately  $200 \text{ g m}^{-2} \text{ year}^{-1}$  from 1960  
231 to 1980, after which a gradual decline in carbon burial was still measured. In relation to  
232 land use/cover in the surroundings of fluvial channels and the Jupindá lake over time,  
233 only the smallest buffer (100 m) showed more intense relative changes during the  
234 previous period 1934-1975, when the increase in deforested area was around 75 % higher  
235 than in the subsequent time period 1975-2008 (Figure 8).

236

237 **4. Discussion**

238 Overall, similar estimates of sediment accretion using different methodologies  
239 (i.e. 60 and 120 year trends from the  $^{239+240}\text{Pu}$  and  $^{210}\text{Pb}_{(\text{ex})}$  models, respectively), along  
240 with the dry bulk revealed an insight into changes in the sediment sources. This indicates  
241 that even though the origin of the sediment may have been modified, the sediment  
242 accumulation has varied little as indicated by the 60- or 120-year sediment accumulation  
243 rates.

244 The high peak in carbon accumulation observed around 1950 appears to be  
245 associated with a shift in the source of organic material, inferred by changes in carbon  
246 and nitrogen contents and the isotopic fractioning toward the middle (from 40 to 20 cm  
247 depth interval) of the sediment column. This peak for different organic and inorganic  
248 variables in intermediate depths revealed changes not only in the amount but also in the  
249 type of material being deposited over time. Previous studies have reported two common  
250 origins for OC in the Amazon forest. Higher  $\delta^{15}\text{N}$  and more negative  $\delta^{13}\text{C}$  values could  
251 indicate the presence of Santarém soil organic matter (such as that adjacent to the Jupindá  
252 Lake), while lower  $\delta^{15}\text{N}$  and more variable  $\delta^{13}\text{C}$  values indicate particulate organic  
253 carbon (POC) from the terrestrial vegetation in the catchment (Ometto et al. 2006,  
254 Zocatelli et al. 2013). Here, a corresponding increase in OC%, TN% and OC burial rates  
255 measured, with a peak near ~1950, suggesting higher inputs of organic matter into lake.  
256 The higher  $\delta^{13}\text{C}$  signature, coupled with a lower  $\delta^{15}\text{N}$  indicates a greater influence from  
257 the terrestrial Amazonian POC during the same period around 1950 (Ometto et al., 2006).

258 The stable isotope results and OC burial rates, when grouped into different  
259 phases, showed assumptions required for parametric analyses, including normal  
260 distribution (Kolmogorov-Smirnov,  $p > 0.05$ ) and homogeneity of variance (Bartlett,  $p >$

261 0.05) (Figure 7). Thus, when examining the means and standard errors to represent the  
262 distribution of values, and parametric tests, different sedimentary phases are noted. These  
263 different sedimentary phases are confirmed by statistical differences as tested using a  
264 one-way ANOVA test followed by Tukey's post test (significance was defined as  $p <$   
265 0.05).

266 When looking for a cause for this change in the source of organic material, we  
267 look to the analysis of land use change. Land clearing associated with early occupation  
268 from the 1940s in the catchment area of the Jupindá Lake reveals a potential cause of the  
269 increased carbon burial observed in this lake. Changes in land use and cover may  
270 significantly affect recent OC burial in mid-high-latitude lakes (Anderson et al. 2013,  
271 Dietz et al. 2015). Our results suggest that land clearing during the 1940's and 50's might  
272 be related to increased organic matter deposition in the region's floodplain lakes. During  
273 this period, intense wood extraction and expansion of agricultural settlements occurred  
274 (Amorim 2000, Cruz et al. 2011). One important consequence of deforestation in the  
275 watershed is the silting up of lakes (Enea et al. 2012 ), including those at humid low-  
276 latitude areas (Cohen et al. 2005, Bakoarinaiaina et al. 2006). The riparian forest systems  
277 are generally effective in reducing the sediment transport by surface runoff, with the  
278 removal of this vegetation increasing the erosion processes especially in the Amazon  
279 basin due to intense rainfall (Neill et al. 2013a). The lake is in a  
280 region relatively preserved, and therefore there is no other explanation other than  
281 deforestation in the margins which may have caused the peak in OC burial found between  
282 1934 and 1975.

283        We also found a spatial dependence of the carbon accumulation in the Lake  
284        Jupindá, as the much lower OC burial was coupled to higher deforestation rates in those  
285        larger buffers around its margins and main fluvial channels (500, 1000 and 6000 m) in  
286        the period after 1975 (1975-2008) than that before (1934-1975). This confirms previous  
287        evidences that the recent deforestation process in the region was started in areas around  
288        running and lake waters (Amorim 2000, Cruz et al. 2011), and not in the interior of the  
289        forest. The enhanced OC burial in lacustrine sediments before 1975 was related to higher  
290        deforestation rates only in the riparian vegetation zone (100-m buffers), suggesting a  
291        higher influence of deforestation with decreasing distance to water courses. Therefore,  
292        the soil carbon enrichment to the aquatic sediments during the peaks of riparian  
293        deforestation may cause intense but temporary carbon burial events in the Amazon  
294        floodplain, representing a significant part of the total loss of terrestrial organic matter. In  
295        contrast, the continued removal of vegetation from the interior of the forest might be not  
296        directly related to increases of OC burial, even temporarily, in depositional aquatic  
297        ecosystems.

298

## 299        **5. Conclusion**

300        The  $^{239+240}\text{Pu}$  and  $^{210}\text{Pb}$  dating methods were combined with a spatial analysis of  
301        vegetation clearing to firstly calculate carbon accumulation rates, and then to interpret  
302        changes in sediment characteristics during the previous century. The Pu dating method  
303        closely approximates measurements from the  $^{210}\text{Pb}$  chronologies and hence offers  
304        mechanism to determine sedimentation rates and carbon accumulation in Amazon  
305        sediments. An increase in OC burial, 150 to  $\sim 300 \text{ OC g m}^{-2} \text{ year}^{-1}$ , coincides with

306 changes in the  $\delta^{13}\text{C}$  and  $\delta^{15}\text{N}$  signatures, likely influenced by the heavy deforestation in  
307 riparian systems of this region during the 1940s and 50's. It is therefore suggested that  
308 the net increase in carbon burial towards the center of the sediment core, which  
309 represents the highest carbon burial rates during the 1950s, is a result of a change in  
310 source of organic matter deposition. The differing carbon burial rates along the sediment  
311 core reveals the potential complexity of carbon burial rates in the Amazon floodplain  
312 lakes, directly related to the development within the Basin. This work demonstrates a  
313 new understanding on spatial dependence of carbon burial capacity of the Amazon  
314 floodplain lakes with respect to advances in deforestation in the basin.

315

316

317 **Acknowledgements**

318 LMS is supported by an APA and IPRS scholarships. HM received a research grant from  
319 the Brazilian Research Council (CNPq – “Programa Universal”) and the Research  
320 Support Foundation of the State of Rio de Janeiro (FAPERJ – “Programa Jovem Cientista  
321 do Nosso Estado”). CJS is supported by the Australian Research Council  
322 (DE150100581).

323

324

325

326

327

328

329

330

331

332

333 **CAPTIONS TO FIGURES**

334 **Figure 1.** Floodplain Lake where the sediment core was collect, near the Amazon River  
335 and the city of Santarém, Brazil. This floodplain lake has a diameter of approximately 3  
336 km.

337 **Figure 2.** Different buffer sizes (100m, 500m, 1km and 6km) along the stretch of the  
338 Curuá-Una river from Jupindá Lake (red) to the hydroelectric dam upstream (yellow).

339 **Figure 3.**  $^{239+240}\text{Pu}$  profile, indicating  $\sim 1950$  when these radionuclides were first  
340 introduced into the atmosphere.

341 **Figure 4.** Lead-210 (black circles) and  $^{226}\text{Ra}$  (white circles) profiles against depth. Grey  
342 squares represent the  $^{210}\text{Pb}(\text{ex})$  profile vs cumulative dry mass.

343 **Figure 5.**  $\delta^{13}\text{C}$  vs  $\delta^{15}\text{N}$ . The Amazon River POM and Santarem soil organic matter  
344 values, adjacent to the study area, are taken from Zocatelli et al (2013).

345 **Figure 6.** Carbon burial as a function of  $\delta^{13}\text{C}$ .

346 **Figure 7.**  $\delta^{13}\text{C}$ ,  $\delta^{15}\text{N}$  and carbon burial rate values in relation to age (year). "Panels  
347 below each vertical profile represent respective data grouped by the phases >1934, 1934-  
348 1975 and 1975-2008. Filled square symbols represent means of a given variable in each  
349 sediment layer, and the vertical bars show the mean with the standard deviation of the  
350 respective phase. Equal letters in each panel represent non-significant differences ( $p >$   
351 0.05, one-way ANOVA followed by Tukey's post test)."

352 **Figure 8.** Percentage of modified areas in relation to the different buffers.

353

354

355

356

357 **CAPTION TO TABLES**

358 **Table 1.** Satellite acquisition data from United States Geological Survey (USGS) and the

359 Curuá-Una River quota from Brazilian Water Agency (ANA).

360 **Table 2.** Depth profiles of dry bulk density (DBD), total organic carbon (OC%), total

361 nitrogen (TN%) carbon and nitrogen (C/N) molar ratios,  $\delta^{13}\text{C}$  and  $\delta^{15}\text{N}$ .

362

363

364

365

366

367

368

369

370

371

372

373

374

375

376

377

378

379

380

381

382

383

384

385

386

387

388

389

390

391  
392  
393  
394  
395  
396  
397  
398  
399  
400  
401  
402 **Table 1.**  
403

<i>Month/Year</i>	<i>Landsat Data</i>	<i>Curuá-Una River</i>
		<i>Quote</i>
Aug/1975	2	5.3
Oct/1985	5	3.7
June/1995	5	6
June/2008	5	<i>No data</i>

404  
405  
406  
407 **Table 2.**  
408

<b>Depth (cm)</b>	<b>DBD (g cm<sup>-3</sup>)</b>	<b><math>\delta^{15}\text{N}</math></b>	<b><math>\delta^{13}\text{C}</math></b>	<b>C (%)</b>	<b>N (%)</b>	<b>C/N</b>
0-2	1.0	8.9	-29.2	3.8	0.3	17.2
2-4	0.9	11.7	-29.0	3.8	0.3	18.7
4-6	1.0	10.4	-28.8	4.0	0.3	19.2
6-8	1.1	9.3	-28.7	4.3	0.3	20.2
8-10	1.0	9.4	-28.7	4.1	0.3	19.8
10-12	1.1	7.9	-28.6	4.6	0.3	21.2
12-14	1.1	8.2	-28.7	4.3	0.3	19.9
14-16	1.1	7.8	-28.6	4.3	0.3	20.9
16-18	1.0	8.7	-28.5	4.4	0.3	21.2
18-20	1.1	7.5	-28.4	4.4	0.3	19.8
20-22	1.0	6.5	-28.2	5.4	0.3	21.2
22-24	1.0	6.0	-27.8	5.3	0.3	21.5
24-26	1.0	5.2	-27.4	7.3	0.4	25.4
26-28	1.1	6.1	-27.6	6.0	0.3	23.8
28-30	1.0	5.0	-27.3	6.0	0.4	22.7
30-32	1.0	5.4	-28.0	6.1	0.3	27.0
32-34	1.3	6.6	-28.5	4.4	0.2	27.5
34-36	1.6	8.9	-29.0	2.2	0.1	23.1
36-38	1.4	11.4	-29.4	2.9	0.1	30.4
38-40	1.4	10.4	-29.5	3.3	0.1	30.5
40-42	1.5	11.4	-29.3	2.4	0.1	23.8
42-44	1.6	12.2	-29.4	1.3	0.1	15.6
44-46	1.8	8.2	-29.6	1.2	0.1	14.3
46-48	1.5	8.8	-29.8	2.2	0.1	21.6

48-50	0.9	10.4	-29.7	2.9	0.2	25.6
50-52	0.9	10.2	-29.7	2.6	0.1	27.2
52-54	0.9	7.1	-29.7	3.9	0.2	28.6
54-56	0.9	9.2	-29.9	3.6	0.2	27.8
56-58	0.9	6.6	-30.1	4.3	0.2	30.1
58-60	0.9	5.0	-30.1	3.5	0.2	23.1
<b>Average</b>	<b>1.11</b>	<b>8.34</b>	<b>-28.9</b>	<b>4.0</b>	<b>0.2</b>	<b>23.0</b>
<b>Stand Dev</b>	<b>0.24</b>	<b>2.1</b>	<b>0.8</b>	<b>1.9</b>	<b>0.1</b>	<b>4.2</b>

409

410

411

412 **References**

413

414 Aalto, R., L. Maurice-Bourgois, T. Dunne, D. R. Montgomery, C. A. Nittrouer, and J. L.  
 415 Guyot. 2003. Episodic sediment accumulation on Amazonian flood plains  
 416 influenced by El Niño/Southern Oscillation. *Nature* **425**:493-497.

417 Abril, G., J. M. Martinez, L. F. Artigas, P. Moreira-Turcq, M. F. Benedetti, L. Vidal, T.  
 418 Meziane, J. H. Kim, M. C. Bernardes, N. Savoye, J. Deborde, E. L. Souza, P.  
 419 Albéric, M. F. Landim De Souza, and F. Roland. 2014. Amazon River carbon  
 420 dioxide outgassing fuelled by wetlands. *Nature* **505**:395-398.

421 Amorim, A. T. d. S. 2000. Santarém: uma síntese histórica, Canoas, Ulbra, Santarem,  
 422 Brazil

423 Anderson, N. J., R. D. Dietz, and D. R. Engstrom. 2013. Land-use change, not climate,  
 424 controls organic carbon burial in lakes. *Proceedings. Biological sciences / The  
 425 Royal Society* **280**:20131278.

426 Appleby, P. G., and F. Oldfield. 1992. Application of lead-210 to sedimentation studies.  
 427 Pages 731-783 *in* M. Ivanovich and S. Harmon, editors. *Uranium Series  
 428 Disequilibrium: Application to Earth, Marine and Environmental Science*. Oxford  
 429 Science Publications.

430 Bakoariniaina, L. N., T. Kusky, and T. Raharimahefa. 2006. Disappearing Lake Alaotra:  
431 Monitoring catastrophic erosion, waterway silting, and land degradation hazards  
432 in Madagascar using Landsat imagery. *Journal of African Earth Sciences* **44**:241-  
433 252.

434 Cohen, A. S., M. R. Palacios-Fest, J. McGill, P. W. Swarzenski, D. Verschuren, R.  
435 Sinyinza, T. Songori, B. Kakagozo, M. Syampila, C. M. O'Reilly, and S. R. Alin.  
436 2005. Paleolimnological investigations of anthropogenic environmental change in  
437 Lake Tanganyika: I. An introduction to the project. *Journal of Paleolimnology*  
438 **34**:1-18.

439 Cruz, H., P. Sablayrolles, M. Kanashiro, and M. S. Amaral, P. 2011. Relação empresa/  
440 comunidade no manejo florestal comunitário e familiar: Uma contribuição do  
441 Projeto Floresta em pé.

442 Diaz, R. J., and R. Rosenberg. 2008. Spreading dead zones and consequences for marine  
443 ecosystems. *Science* **321**:926-929.

444 Dietz, R. D., D. R. Engstrom, and N. J. Anderson. 2015. Patterns and drivers of change in  
445 organic carbon burial across a diverse landscape: Insights from 116 Minnesota  
446 lakes. *Global Biogeochemical Cycles* **29**:708-727.

447 Dong, X., N. J. Anderson, X. Yang, X. chen, and J. Shen. 2012. Carbon burial by shallow  
448 lakes on the Yangtze floodplain and its relevance to regional carbon sequestration.  
449 *Global Change Biology* **18**:2205-2217.

450 Downing, J. P., M. Meybeck, J. C. Orr, R. R. Twilley, and H. W. Scharpenseel. 1993.  
451 Land and water interface zones. *Water, Air, & Soil Pollution* **70**:123-137.

452 Enea, A., G. Romanescu, and C. Stoleriu. 2012 Quantitative considerations concerning  
453 the source-areas for the silting of the red lake (Romania) lacustrine basin.  
454 . Romania.

455 Fearnside, P. M. 2005. Do hydroelectric dams mitigate global warming? The case of  
456 Brazil's Curuá-Una Dam. *Mitigation and Adaptation Strategies for Global Change*  
457 **10**:675-691.

458 Gordon, S. I. 1980. Utilizing LANDSAT imagery to monitor land-use change: A case  
459 study in ohio. *Remote Sensing of Environment* **9**:189-196.

460 Goulding, M. 1993. Flooded forests of the Amazon. *Scientific American* **268**:114-  
461 120+115.

462 Hoffmann, T., M. Schlummer, B. Notebaert, G. Verstraeten, and O. Korup. 2013. Carbon  
463 burial in soil sediments from Holocene agricultural erosion, Central Europe.  
464 *Global Biogeochemical Cycles* **27**:828-835.

465 INPE. 2016. Program for the Estimation of Amazon Deforestation. Accessed 20  
466 November 2016, [http://www.obt.inpe.br/prodes/prodes\\_1988\\_2015n.htm](http://www.obt.inpe.br/prodes/prodes_1988_2015n.htm).

467 Ivanovich, M., and S. Harmon. 1992. *Uranium Series Disequilibrium - Applications to*  
468 *Earth, Marine and Environmental Sciences*. second edition edition. Oxford  
469 *Science Publications*.

470 Junk, W. J. 2013. Current state of knowledge regarding South America wetlands and  
471 their future under global climate change. *Aquatic Sciences* **75**:113-131.

472 Ketterer, M. E., K. M. Hafer, V. J. Jones, and P. G. Appleby. 2004. Rapid dating of  
473 recent sediments in Loch Ness: Inductively coupled plasma mass spectrometric

474 measurements of global fallout plutonium. *Science of the Total Environment*  
475 **322**:221-229.

476 LigockI, L. P. 2003. Comportamento geotécnico da barragem de Curuá-Una, Pará. Rio de  
477 Janeiro.

478 Lucas, C. M., J. Schöngart, P. Sheikh, F. Wittmann, M. T. F. Piedade, and D. G.  
479 McGrath. 2014. Effects of land-use and hydroperiod on aboveground biomass and  
480 productivity of secondary Amazonian floodplain forests. *Forest Ecology and  
481 Management* **319**:116-127.

482 Marotta, H., L. Bento, F. A. De Esteves, and A. Enrich-Prast. 2009. Whole ecosystem  
483 evidence of eutrophication enhancement by wetland dredging in a shallow  
484 Tropical Lake. *Estuaries and Coasts* **32**:654-660.

485 Marotta, H., C. M. Duarte, F. Meirelles-Pereira, L. Bento, F. A. Esteves, and A. Enrich-  
486 Prast. 2010. Long-term CO<sub>2</sub> variability in two shallow tropical lakes experiencing  
487 episodic eutrophication and acidification events. *Ecosystems* **13**:382-392.

488 Marotta, H., L. Pinho, C. Gudasz, D. Bastviken, L. J. Tranvik, and A. Enrich-Prast. 2014.  
489 Greenhouse gas production in low-latitude lake sediments responds strongly to  
490 warming. *Nature Climate Change* **4**:467-470.

491 Melack, J. M., L. L. Hess, M. Gastil, B. R. Forsberg, S. K. Hamilton, I. B. T. Lima, and  
492 E. M. L. M. Novo. 2004. Regionalization of methane emissions in the Amazon  
493 Basin with microwave remote sensing. *Global Change Biology* **10**:530-544.

494 Munyati, C. 2000. Wetland change detection on the Kafue Flats, Zambia, by  
495 classification of a multitemporal remote sensing image dataset. *International  
496 Journal of Remote Sensing* **21**:1787-1806.

497 Neill, C., M. T. Coe, S. H. Riskin, A. V. Krusche, H. Elsenbeer, M. N. Macedo, R.

498 McHorney, P. Lefebvre, E. A. Davidson, R. Scheffler, A. M. e Silva Figueira, S.

499 Porder, and L. A. Deegan. 2013a. Watershed responses to Amazon soya bean

500 cropland expansion and intensification. *Philosophical Transactions of the Royal*

501 *Society B: Biological Sciences* **368**.

502 Neill, C., M. T. Coe, S. H. Riskin, A. V. Krusche, H. Elsenbeer, M. N. Macedo, R.

503 McHorney, P. Lefebvre, E. A. Davidson, R. Scheffler, A. M. Figueira, S. Porder,

504 and L. A. Deegan. 2013b. Watershed responses to Amazon soya bean cropland

505 expansion and intensification. *Philosophical transactions of the Royal Society of*

506 *London. Series B, Biological sciences* **368**:20120425.

507 Neue, H. U., J. L. Gaunt, Z. P. Wang, P. Becker-Heidmann, and C. Quijano. 1997.

508 Carbon in tropical wetlands. *Geoderma* **79**:163-185.

509 Ometto, J. P. H. B., J. R. Ehleringer, T. F. Domingues, J. A. Berry, F. Y. Ishida, E.

510 Mazzi, N. Higuchi, L. B. Flanagan, G. B. Nardoto, and L. A. Martinelli. 2006.

511 The stable carbon and nitrogen isotopic composition of vegetation in tropical

512 forests of the Amazon Basin, Brazil. *Biogeochemistry* **79**:251-274.

513 Peixoto, R. B., H. Marotta, D. Bastviken, and A. Enrich-Prast. 2016. Floating Aquatic

514 Macrophytes Can Substantially Offset Open Water CO<sub>2</sub> Emissions

515 from Tropical Floodplain Lake Ecosystems. *Ecosystems* **19**:724-736.

516 Sanders, C. J., B. D. Eyre, I. R. Santos, W. MacHado, W. Luiz-Silva, J. M. Smoak, J. L.

517 Breithaupt, M. E. Ketterer, L. Sanders, H. Marotta, and E. Silva-Filho. 2014.

518 Elevated rates of organic carbon, nitrogen, and phosphorus accumulation in a

519 highly impacted mangrove wetland. *Geophysical Research Letters* **41**:2475-2480.

520 Sanders, C. J., I. R. Santos, D. T. Maher, J. L. Breithaupt, J. M. Smoak, M. Ketterer, M.  
521 Call, L. Sanders, and B. D. Eyre. 2016. Examining 239+240Pu, 210Pb and  
522 historical events to determine carbon, nitrogen and phosphorus burial in  
523 mangrove sediments of Moreton Bay, Australia. *Journal of Environmental  
524 Radioactivity* **151**:623-629.

525 Skole, D., and C. Tucker. 1993. Tropical deforestation and habitat fragmentation in the  
526 amazon: Satellite data from 1978 to 1988. *Science* **260**:1905-1910.

527 Smith, L. K., J. M. Melack, and D. E. Hammond. 2002. Carbon, nitrogen, and  
528 phosphorus content and 210Pb-derived burial rates in sediments of an Amazon  
529 floodplain lake. *Amazoniana* **17**:413-436.

530 Stanley, E. H., S. M. Powers, N. R. Lottig, I. Buffam, and J. T. Crawford. 2012.  
531 Contemporary changes in dissolved organic carbon (DOC) in human-dominated  
532 rivers: Is there a role for DOC management? *Freshwater Biology* **57**:26-42.

533 Zocatelli, R., P. Moreira-Turcq, M. Bernardes, B. Turcq, R. C. Cordeiro, S. Gogo, J. R.  
534 Disnar, and M. Boussafir. 2013. Sedimentary evidence of soil organic matter  
535 input to the curuai amazonian floodplain. *Organic Geochemistry* **63**:40-47.

536

537

538

539

540

541

542

543

544

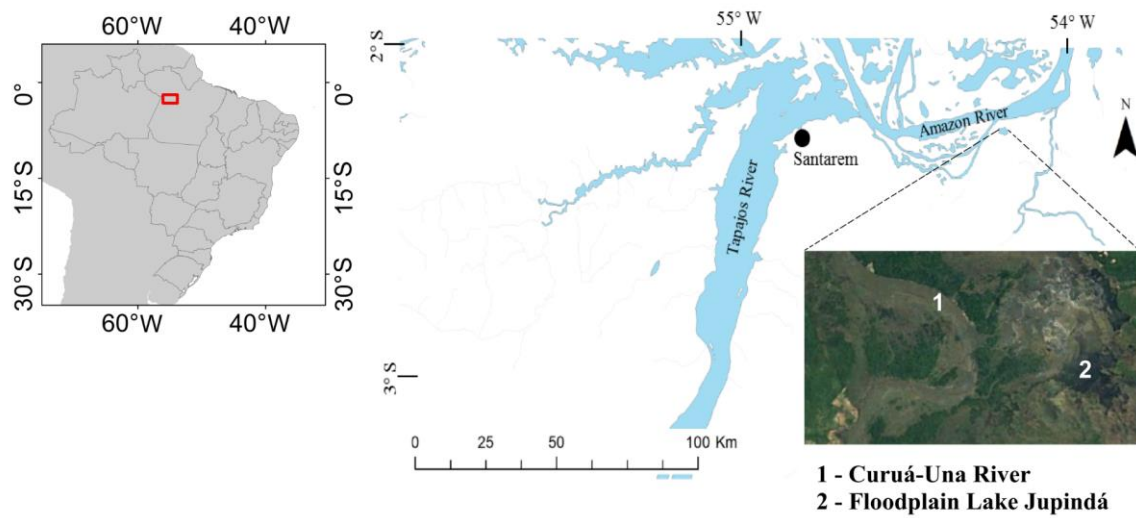
545

546

547

548

549 **Figure 1.**



550

551

552

553

554

555

556

557

558

559

560

561

562

563

564

565

566

567

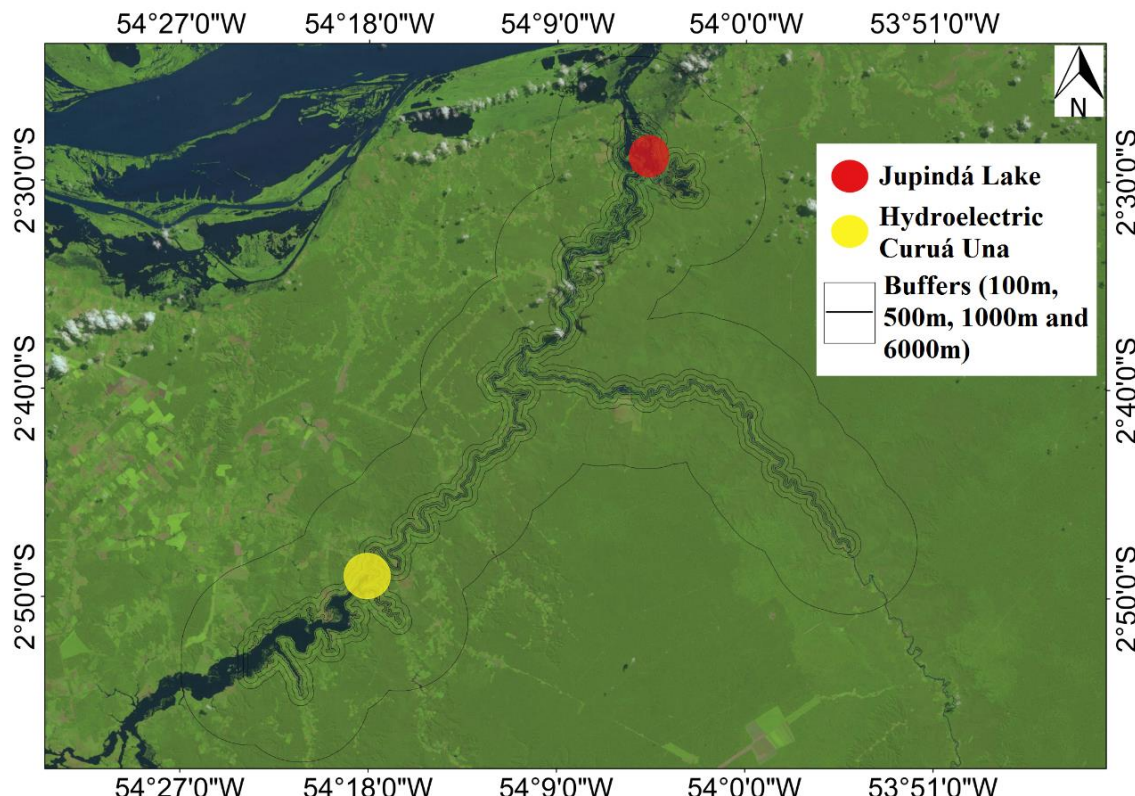
568

569

570

571  
572  
573  
574  
575  
576  
577  
578  
579  
580  
581

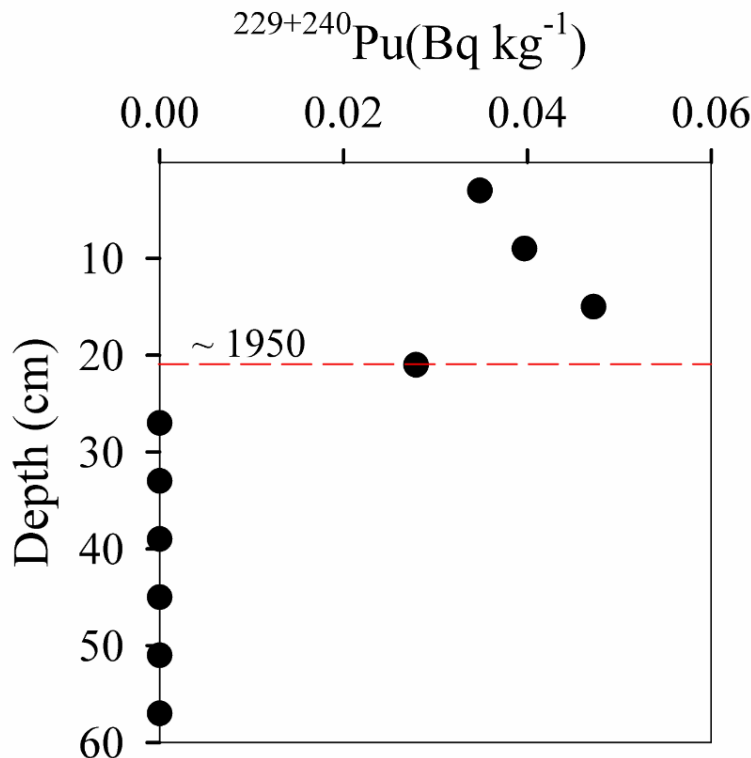
**Figure 2.**



582  
583  
584  
585  
586  
587  
588  
589  
590  
591  
592  
593  
594  
595

596  
597  
598  
599  
600  
601  
602  
603  
604  
605  
606

**Figure 3.**

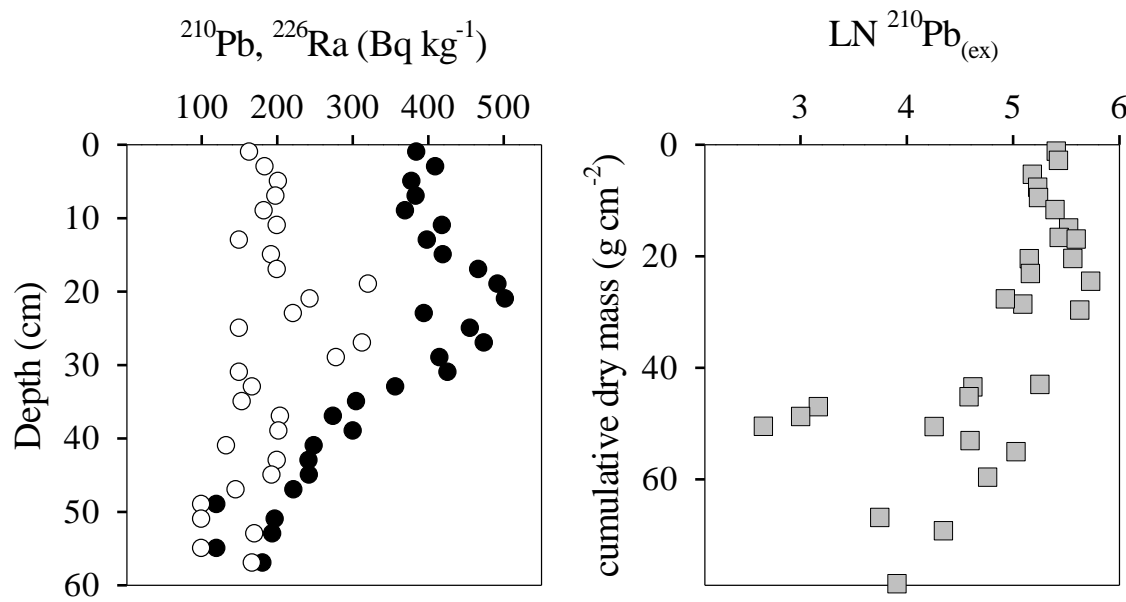


607  
608  
609  
610  
611  
612  
613  
614  
615  
616  
617  
618  
619  
620

621  
622  
623  
624  
625  
626  
627  
628  
629  
630  
631

**Figure 4.**

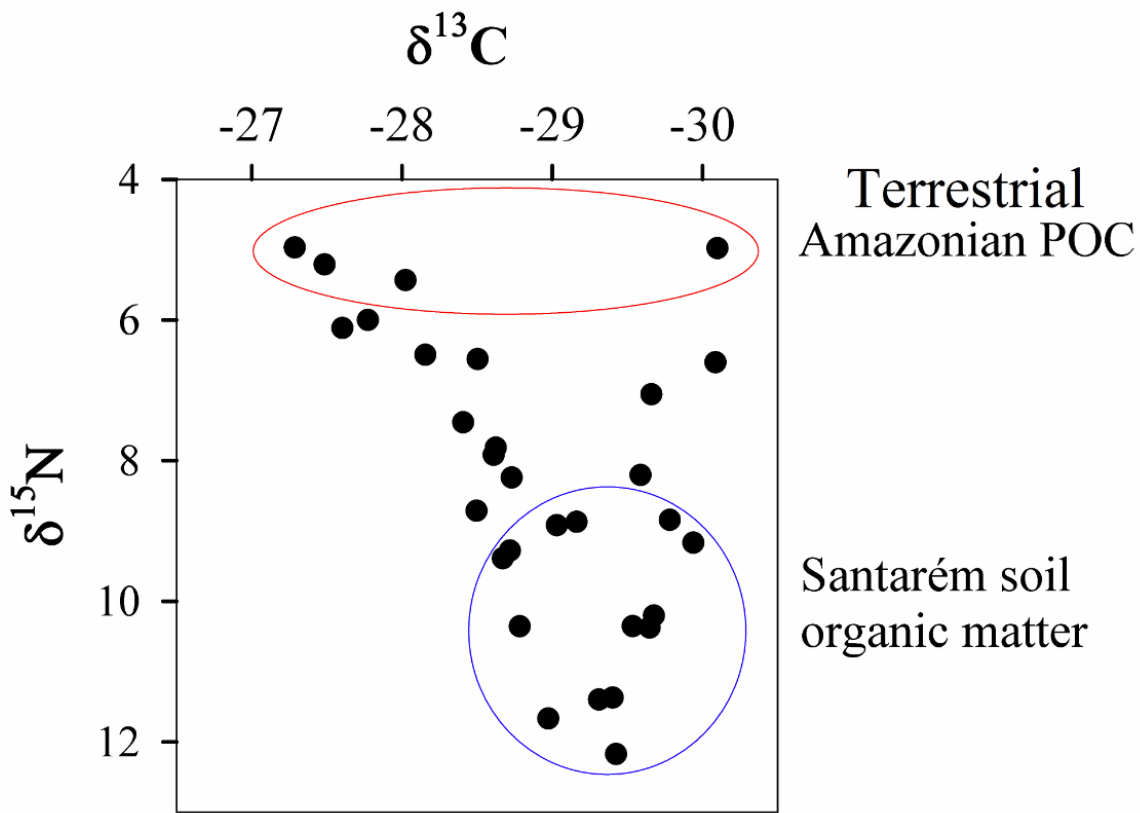
632



633  
634  
635  
636  
637  
638  
639  
640  
641  
642  
643  
644  
645  
646  
647  
648  
649  
650  
651

652  
653  
654  
655  
656  
657  
658  
659  
660  
661  
662

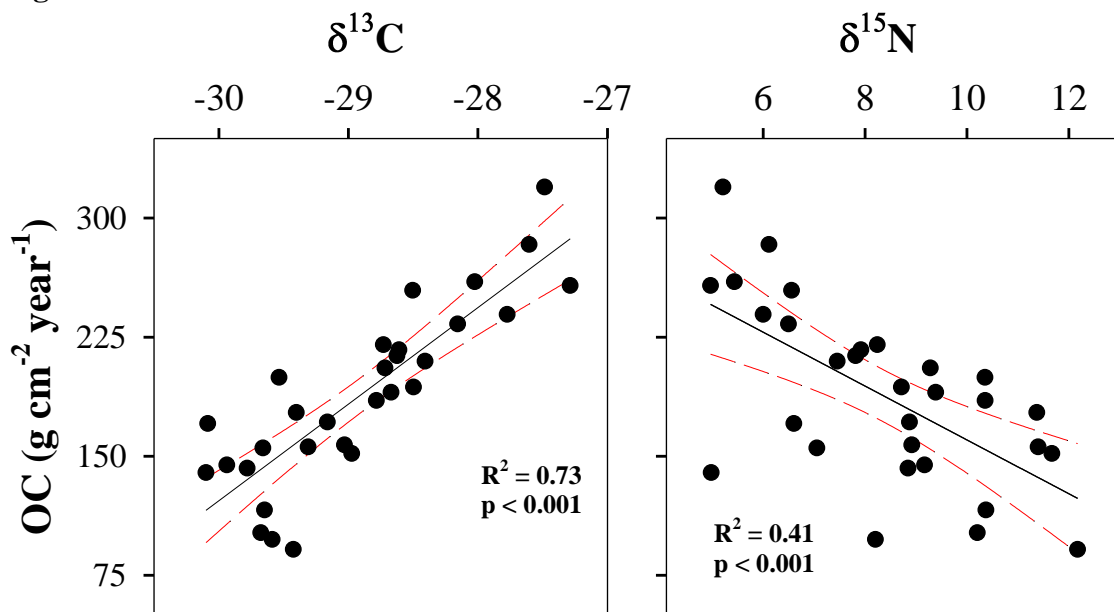
**Figure 5.**



663  
664  
665  
666  
667  
668  
669  
670  
671  
672  
673  
674  
675

676  
677  
678  
679  
680  
681  
682  
683  
684  
685  
686

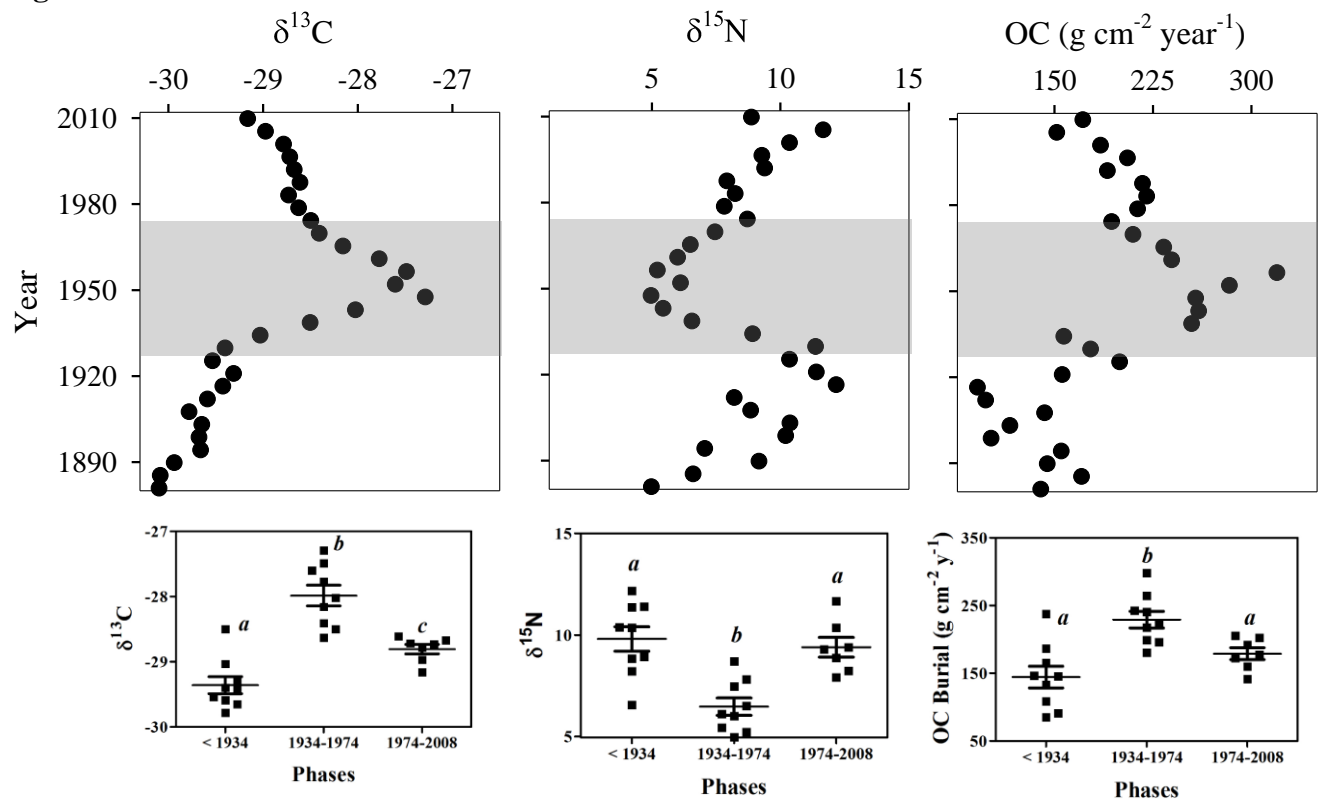
**Figure 6.**



687  
688  
689  
690  
691  
692  
693  
694  
695  
696  
697  
698  
699  
700  
701  
702  
703

704  
705  
706  
707  
708  
709  
710  
711  
712  
713  
714

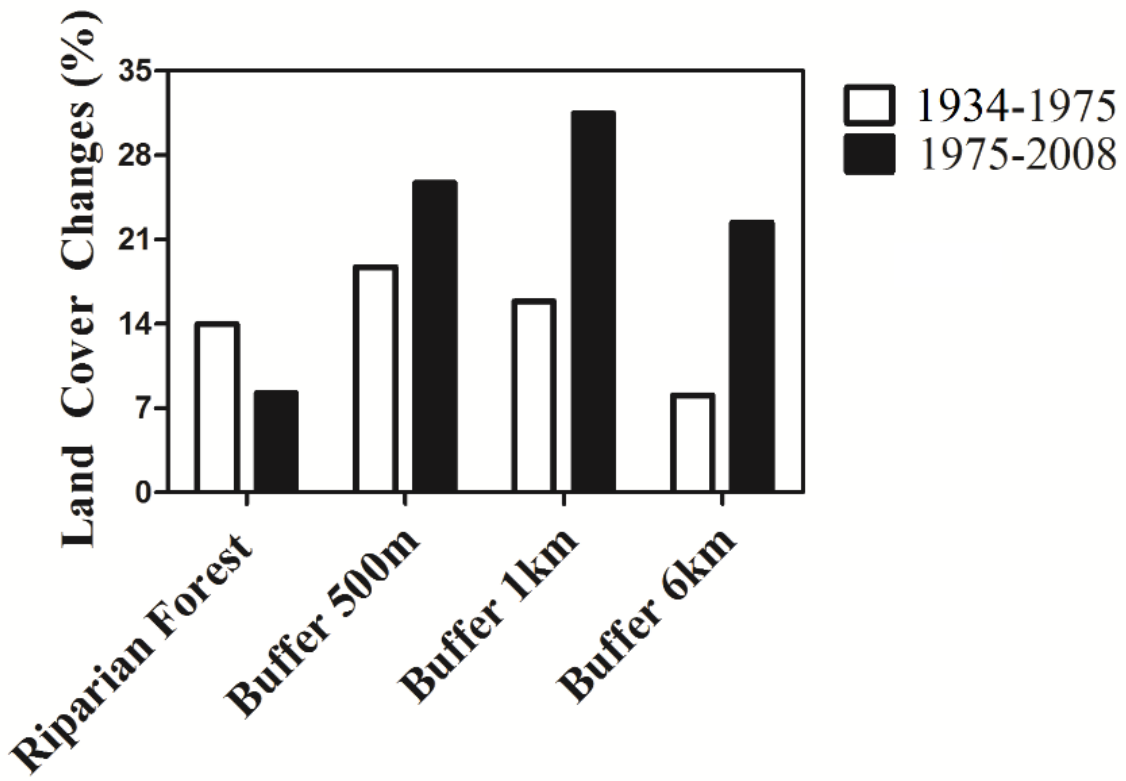
**Figure 7.**



715  
716  
717  
718  
719  
720  
721  
722  
723  
724  
725  
726  
727  
728  
729

730  
731  
732  
733  
734  
735  
736  
737  
738  
739  
740

**Figure 8.**



741